

Structural and biochemical insights into the role of testis-expressed gene 14 (TEX14) in forming the stable intercellular bridges of germ cells

Hee Jung Kim^{a,1}, Jungbin Yoon^{b,1}, Atsushi Matsuura^a, Jung-Hyun Na^a, Won-Kyu Lee^a, Hyunook Kim^c, Ji Woong Choi^d, Ji Eun Park^e, Sung-Jean Park^e, Kyung Tae Kim^f, Rakwoo Chang^c, Byung Il Lee^d, Yeon Gyu Yu^a, Yeon-Kyun Shin^{g,h}, Chelhyun Jeong^g, Kunsoo Rhee^b, and Hyung Ho Lee^{i,2}

^aDepartment of Bio & Nano Chemistry, Kookmin University, Seoul 136-702, Korea; ^bDepartment of Biological Sciences, Seoul National University, Seoul 151-747, Korea; ^cDepartment of Chemistry, Kwangwoon University, Seoul 139-701, Korea; ^dBiomolecular Function Research Branch, Division of Convergence Technology, National Cancer Center, Goyang, Gyeonggi 416-769, Korea; ^eCollege of Pharmacy, Gachon University, Incheon 406-799, Korea; ^fMolecular Epidemiology Branch, Division of Cancer Epidemiology and Prevention, National Cancer Center, Goyang, Gyeonggi 416-769, Korea; ^gCenter for Theragnosis, Biomedical Research Institute, Korean Institute of Science and Technology, Seoul 136-791, Korea; ^hDepartment of Biochemistry, Biophysics, and Molecular Biology, Iowa State University, Ames, IA 50011; and ⁱDepartment of Chemistry, College of Natural Sciences, Seoul National University, Seoul 151-742, Korea

Edited by Wesley I. Sundquist, University of Utah School of Medicine, Salt Lake City, UT, and approved August 28, 2015 (received for review September 26, 2014)

Intercellular bridges are a conserved feature of spermatogenesis in mammalian germ cells and derive from arresting cell abscission at the final stage of cytokinesis. However, it remains to be fully understood how germ cell abscission is arrested in the presence of general cytokinesis components. The TEX14 (testis-expressed gene 14) protein is recruited to the midbody and plays a key role in the inactivation of germ cell abscission. To gain insights into the structural organization of TEX14 at the midbody, we have determined the crystal structures of the EABR [endosomal sorting complex required for transport (ESCRT) and ALIX-binding region] of CEP55 bound to the TEX14 peptide (or its chimeric peptides) and performed functional characterization of the CEP55–TEX14 interaction by multiexperiment analyses. We show that TEX14 interacts with CEP55-EABR via its AxGPPx₃Y (Ala793, Gly795, Pro796, Pro797, and Tyr801) and PP (Pro803 and Pro804) sequences, which together form the AxGPPx₃YxPP motif. TEX14 competitively binds to CEP55-EABR to prevent the recruitment of ALIX, which is a component of the ESCRT machinery with the AxGPPx₃Y motif. We also demonstrate that a high affinity and a low dissociation rate of TEX14 to CEP55, and an increase in the local concentration of TEX14, cooperatively prevent ALIX from recruiting ESCRT complexes to the midbody. The action mechanism of TEX14 suggests a scheme of how to inactivate the abscission of abnormal cells, including cancer cells.

TEX14 | intercellular bridges | CEP55 | germ cells | cytokinesis

Intercellular bridges are a distinct feature of spermatogenesis in mammalian germ cells. Although observations of intercellular bridges were reported more than 100 y ago, their molecular function is largely unknown and we have only recently begun to learn how they form at the molecular level. Interestingly, stable bridges have recently been recognized as providing a unique means of intercellular communication, because cytoplasmic molecules can pass through them (1). The loss of germ cell intercellular bridges disrupts spermatogenesis and causes sterility (2).

The most direct method of cell-to-cell communication is to connect the separate cytosols of cells using a tunnel that allows macromolecules to pass from one cell to another. Various organisms achieve this type of direct intercellular transfer using tunneling nanotubes (3), intercellular bridges (also called ring canals) (1), and bacterial intercellular nanotubes (4). Somatic ring canals have also been found to equilibrate the levels of some proteins between connected cells in invertebrates such as *Drosophila* (5). Among these mechanisms, it has been shown that intercellular bridges having channels that are 0.5–3 μm in diameter are formed by the arrest of cell abscission at the final stage of cytokinesis in the germ cells of vertebrates (1).

Whether the process of cell abscission is completed or not depends on the cell type. In the somatic cells of vertebrates, cell

abscission occurs at the midbody (6), a structure that tethers two daughter cells. The midbody protein CEP55 plays a key role in recruiting the ALIX–endosomal sorting complex required for transport (ESCRT) I complex to the midbody (7, 8). After this event, ESCRT-III subunits, which have a membrane scission activity, are recruited (9–13). Alternatively, to inactivate cell abscission, TEX14, a testis-expressed gene and germ cell-specific component, is recruited to the midbody. It is essential for intercellular bridges and fertility in male mice (2), and has recently been identified as one of the susceptibility genes for testicular germ cell tumors (14).

In germ cells, intercellular bridges are formed throughout spermatogenesis and the arrest of cell abscission is controlled precisely by a sophisticated interplay among the proteins TEX14, ALIX, TSG101 (expressed by tumor susceptibility gene 101; *TSG101*), and CEP55. Therefore, it is important to investigate how TEX14 safeguards intercellular bridges from the potentially damaging membrane scissor in germ cells. To understand the molecular mechanisms involved in this process, we have performed both structural and functional analyses of the CEP55–TEX14 interaction.

Significance

Germ cells possess the inherent ability to inactivate cell abscission through TEX14 (testis-expressed gene 14), and they may provide information on inactivation of the abscission in abnormal cells, including cancer cells. Structural and functional studies of how TEX14 inactivates germ cell abscission reveal that the AxGPPx₃YxPP motif of TEX14 competitively binds to CEP55-EABR [endosomal sorting complex required for transport (ESCRT) and ALIX-binding region] to prevent the recruitment of ALIX, which is a component of the ESCRT machinery and which contains the AxGPPx₃Y motif. Multiexperiment analyses of CEP55-EABR–TEX14 interactions showed how the TEX14 peptide binds dominantly to CEP55-EABR in the presence of ALIX and safeguards the intercellular bridges of germ cells.

Author contributions: H.H.L. designed research; H.J.K., J.Y., A.M., J.-H.N., W.-K.L., H.K., J.W.C., J.E.P., S.-J.P., K.T.K., R.C., B.I.L., Y.G.Y., C.J., and H.H.L. performed research; H.J.K., J.Y., A.M., J.-H.N., W.-K.L., H.K., J.W.C., J.E.P., S.-J.P., K.T.K., R.C., B.I.L., Y.G.Y., Y.-K.S., C.J., K.R., and H.H.L. analyzed data; and K.R. and H.H.L. wrote the paper.

The authors declare no conflict of interest.

This article is a PNAS Direct Submission.

Freely available online through the PNAS open access option.

Data deposition: Crystallography, atomic coordinates, and structure factors have been deposited in the Protein Data Bank, www.pdb.org (PDB ID codes 3WUT, 3WUU, and 3WUV).

¹H.J.K. and J.Y. contributed equally to this work.

²To whom correspondence should be addressed. Email: hyungholee@snu.ac.kr.

This article contains supporting information online at www.pnas.org/lookup/suppl/doi:10.1073/pnas.1418606112/-DCSupplemental.

Results and Discussion

Crystal Structure of CEP55-EABR in Complex with TEX14. In our surface plasmon resonance (SPR) experiment, CEP55-EABR bound to a 13-residue peptide of TEX14 with a dissociation constant (K_d) of ~ 300 nM (Fig. 1 *A–C* and Fig. S1), confirming that this peptide has a higher affinity than ALIX and TSG101 (1–3 μ M) (15). Competitive binding experiments using increasing amounts of the TEX14 peptide demonstrate that TEX14 and ALIX peptides bind to the same site of CEP55-EABR (Fig. 1 *D* and *E*). Previously, we have shown that ALIX and TSG101 compete for the same site on CEP55-EABR (15). Therefore, we conclude that all three peptides (TEX14, ALIX, and TSG101) compete for binding to CEP55-EABR. To gain further insight into the structural organization of TEX14 at the midbody, we have determined the 2.3-Å resolution structure of CEP55-EABR bound to the TEX14 peptide (Fig. 1*F* and Table S1). CEP55-EABR forms a parallel coiled coil over the entire length (Fig. S1*B*) and comprises seven heptad repeats (Fig. 1*F* and Fig. S1*D*). Additionally, one TEX14 peptide was bound to the same binding site as ALIX (15), with a stoichiometry of 2:1 CEP55-EABR:TEX14 (Fig. 1*F* and *G* and Fig. S1*E*). The TEX14 peptide interacts with CEP55-EABR via its AxGPPx₃Y (Ala793,

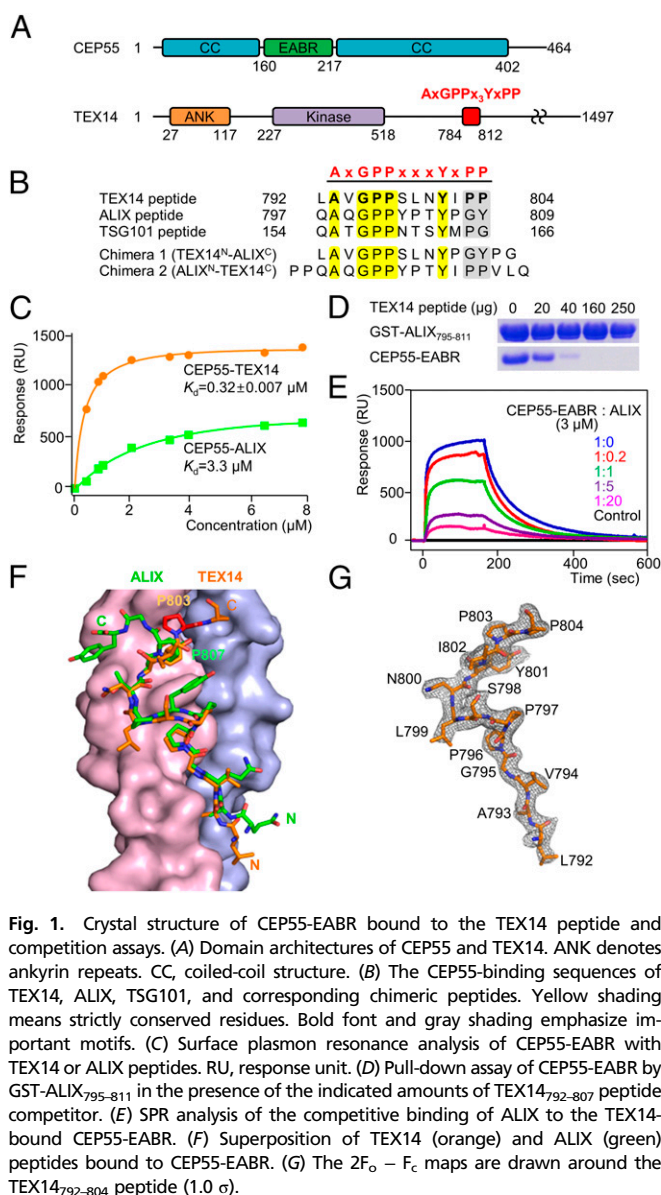


Fig. 1. Crystal structure of CEP55-EABR bound to the TEX14 peptide and competition assays. (A) Domain architectures of CEP55 and TEX14. ANK denotes ankyrin repeats. CC, coiled-coil structure. (B) The CEP55-binding sequences of TEX14, ALIX, TSG101, and corresponding chimeric peptides. Yellow shading means strictly conserved residues. Bold font and gray shading emphasize important motifs. (C) Surface plasmon resonance analysis of CEP55-EABR with TEX14 or ALIX peptides. RU, response unit. (D) Pull-down assay of CEP55-EABR by GST-ALIX_{795–811} in the presence of the indicated amounts of TEX14_{792–807} peptide competitor. (E) SPR analysis of the competitive binding of ALIX to the TEX14-bound CEP55-EABR. (F) Superposition of TEX14 (orange) and ALIX (green) peptides bound to CEP55-EABR. (G) The $2F_o - F_c$ maps are drawn around the TEX14_{792–804} peptide (1.0 σ).

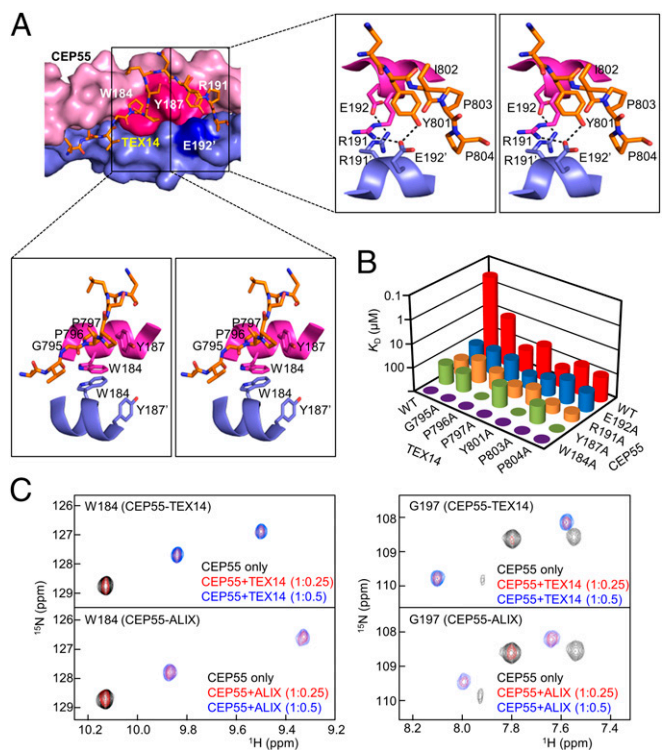


Fig. 2. CEP55-EABR and its interactions with TEX14 (or ALIX). (A) Close-up views of selected regions of the CEP55-EABR surface with the TEX14 peptide. (B) SPR analysis of wild-type and mutant constructs affecting CEP55-EABR binding to TEX14 fragments. (C) Selected regions of the NMR ^1H - ^{15}N TROSY spectra (Fig. S4*A* and *B*) obtained for ^{15}N -labeled CEP55-EABR in the free state (black) and in a complex with TEX14 or ALIX peptides at molar ratios of 1:0.25 (red) and 1:0.5 (blue).

Gly795, Pro796, Pro797, and Tyr801) and PP (Pro803 and Pro804) sequences, which together form the AxGPPx₃YxPP motif (Fig. 1*B*, *F*, and *G* and Fig. S1).

Mutational Studies of the CEP55-EABR–TEX14 Complex. To evaluate the contributions of interfacial residues of the CEP55-EABR–TEX14 complex, the interfacial residues were substituted by Ala and their interactions were examined using SPR. The N terminus of the TEX14 peptide is kinked between the GPP motif and Tyr801, wrapping around the Tyr187 residue of CEP55-EABR; the mutation Y187A reduced the binding affinity to the TEX14 peptide (K_d 149.1 μ M) (Fig. 2*A* and *B* and Figs. S2 and S3). The GPP sequence makes extensive contacts with Trp184 and Tyr187 and with the aliphatic portions of the Lys180 and Gln183 side chains of CEP55-EABR (Fig. 2*A*). Mutation of CEP55-EABR Trp184 almost abolished the binding interaction (Fig. 2*B*). Pro796 and Pro797 make extensive contacts with CEP55-EABR (Fig. 2*A*), and mutation of these residues to Ala significantly reduced binding (K_d 116.1 and 40.4 μ M, respectively) (Fig. 2*B* and Figs. S2 and S3). Moreover, the G795A mutation of TEX14 reduced binding by a factor of ~ 10 (Fig. 2*B* and Figs. S2 and S3). TEX14 Tyr801 (the residue corresponding to Tyr806 on ALIX) also contributes to the binding by forming a strong hydrogen bond (2.8 Å) with the OE1 atom of Glu192' (the prime denotes a residue from the neighboring subunit) (Fig. 2*A*). Mutations of Tyr801 and Glu192' to Ala also reduced the binding interaction (K_d 184.3 and 119.2 μ M, respectively) (Fig. 2*B* and Figs. S2 and S3). Mutation of Arg191 of CEP55 to Ala, which results in severe impairment of the midbody localization of ALIX (15), also abolished the binding to TEX14 (K_d 222.3 μ M) (Fig. 2*B* and Figs. S2 and S3). Double mutations of CEP55-EABR and TEX14 resulted in a greater reduction in affinity than did each single mutation (Fig. 2*B* and Figs. S2 and S3).

Tyr187 of CEP55-EABR makes extensive contacts with Pro796, Tyr801, and Pro804 of the TEX14 peptide (Fig. 2A), and double mutants containing a Y187A/P796A, Y187A/Y801A, and Y187A/P804A of CEP55-EABR–TEX14 mutants (Fig. 2B and Figs. S2 and S3), implying that binding of the TEX14 peptide around Tyr187 of CEP55-EABR is crucial for the interaction between CEP55-EABR and TEX14.

Different Conformations of C-Terminal Tails of TEX14, or ALIX, Peptides.

The overall conformation of the TEX14 peptide is similar to that of the ALIX peptide (15), except the C-terminal residues (Fig. 1F). When the structure of the CEP55-EABR–TEX14 complex is superimposed on that of the CEP55-EABR–ALIX complex, the C-terminal tails of TEX14 and ALIX peptides point in opposite directions (Fig. 1F).

To confirm the conformational difference in the C-terminal tails of TEX14 (or ALIX) peptides in solution, we measured ^{15}N - ^1H heteronuclear single-quantum coherence (HSQC) spectra of CEP55-EABR in the presence of increasing amounts of TEX14 (or ALIX) peptides. Fifty-four (or 46) resonance peaks were perturbed for the CEP55-EABR–TEX14 (or CEP55-EABR–ALIX) complex (Fig. S4). The perturbation peaks showed patterns indicative of high portions of separate peak migrations (89% and 98% slow exchanges for CEP55-EABR–TEX14 and CEP55-EABR–ALIX complexes, respectively), indicating that the overall interaction was slow in terms of chemical exchanges (Fig. S4). Single peaks of CEP55 Trp184 making strong contacts with Val794, Gly795, and Pro796 of TEX14 (or Gln799, Gly800, and Pro801 of ALIX) were split with separate migrations in both CEP55-EABR–TEX14 and CEP55-EABR–ALIX complexes, indicating that the environments of Trp184 and Trp184' were asymmetric when bound to TEX14 or ALIX peptides (Fig. 2C). Chemical shifts of Gly197 and Gly197' residues, which reside near the C terminus of TEX14 or ALIX peptides (9–13 Å apart), also differ (Fig. 2C), indicating that the C-terminal tails of TEX14 and ALIX peptides bind to CEP55-EABR in different ways (Fig. 1F).

The Roles of Pro Residues in the Different Conformations of C-Terminal Tails of TEX14, or ALIX, Peptides.

We next investigated what determines the different conformations of C-terminal tails of TEX14 (or ALIX) peptides. Interestingly, Pro807 of ALIX is found right after Tyr806; however, in TEX14, one additional residue (Ile802) is inserted between Tyr801 (the corresponding residue of ALIX Tyr806) and Pro803 (Fig. 1F). A tyrosine residue increases the tendency of the Pro residue in the Tyr-Pro sequence to take on a *cis* conformation (16). However, the Pro807 residue of ALIX adopts a *trans* conformation (Fig. 1F). All other Pro residues of ALIX and TEX14 peptides also adopt a *trans* conformation (Figs. 1F and 2A). To further investigate the roles of Pro residues (Pro803 of TEX14 and Pro807 of ALIX) in determining the direction of the C terminus, we speculated that the C-terminal conformation could be changed by altering the relative positions of the Pro residues. To investigate this hypothesis, we designed two chimeric peptides (TEX14^N-ALIX^C and ALIX^N-TEX14^C): N-terminal TEX14 (residues 792–801) linked to C-terminal ALIX (residues 807–811) and N-terminal ALIX (residues 795–806) linked to C-terminal TEX14 (residues 802–807) (Fig. 1B). GST pull-down and SPR experiments showed that both TEX14^N-ALIX^C and ALIX^N-TEX14^C peptides bound to CEP55-EABR with lower affinities than those of wild-type TEX14 or ALIX peptides (K_d 7.3 and 6.7 μM , respectively) (Fig. 3A and B). Indeed, crystal structures of CEP55-EABR in complex with TEX14^N-ALIX^C or ALIX^N-TEX14^C peptides show that their C-terminal directions are changed, demonstrating the role of the Pro residues (Fig. 3C–E).

The Dominant Binding of TEX14 to CEP55-EABR Is Achieved by an Increase in the Local Concentration of TEX14 at the Midbody. In somatic cells, TEX14 is not expressed, so that ALIX (or TSG101) may dominate binding to CEP55-EABR (1). In contrast, the

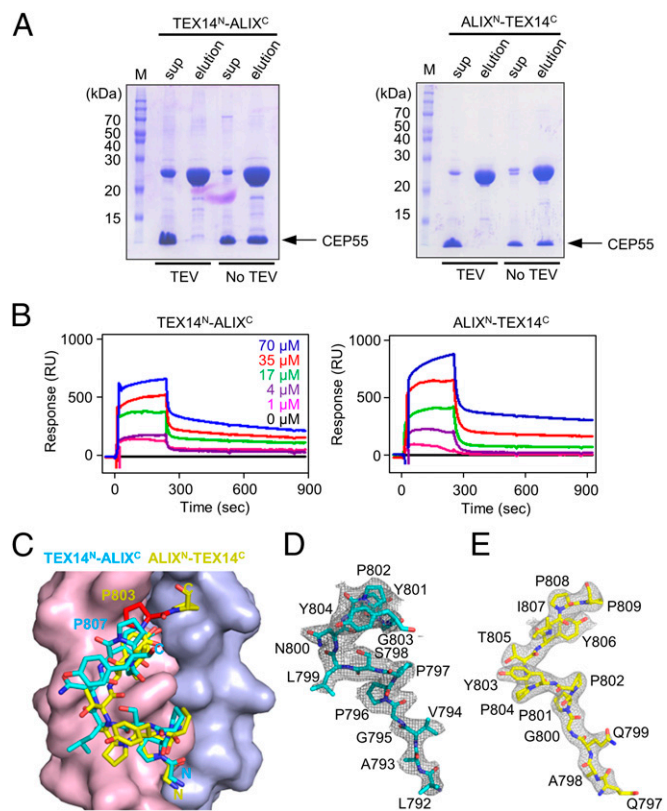


Fig. 3. Crystal structures of CEP55-EABR bound to the chimeric peptides. (A) GST pull-down analysis for the interaction between CEP55-EABR and chimeric peptides. Proteins separated on each gel were visualized by Coomassie blue staining. Each construct is described above the relevant gel image, and arrows indicate the CEP55_{160–217} bound to the GST resin containing GST-TEX14^N-ALIX^C or GST-ALIX^N-TEX14^C. M, protein marker. (B) SPR sensorgrams of CEP55-EABR chimera (GST-TEX14^N-ALIX^C and GST-ALIX^N-TEX14^C) interactions. All sensorgrams were measured by passing the indicated amounts of CEP55_{160–217} protein over flow cells coupled to GST-TEX14^N-ALIX^C or GST-ALIX^N-TEX14^C. (C) Superposition of TEX14^N-ALIX^C (cyan) and ALIX^N-TEX14^C (yellow). (D and E) The 2F_o - F_c maps are drawn around the TEX14^N-ALIX^C peptide (1.0 σ) and ALIX^N-TEX14^C peptide (1.0 σ), respectively.

dominant binding of TEX14 to CEP55-EABR in germ cells needs to be precisely controlled, because both ALIX and TSG101 are expressed in germ cells, as well as TEX14, as shown in our analysis by quantitative real-time reverse transcription-PCR (qRT-PCR) (Fig. 4A and Fig. S4C). Therefore, we next investigated the mechanism by which TEX14 dominantly binds to CEP55 in germ cells in the presence of its competitors (ALIX or TSG101). We hypothesized that the dominant binding of TEX14 to CEP55-EABR in the presence of ALIX (or TSG101) could be achieved by a differential and temporal recruitment to the midbody. This hypothesis is based on the observation that TEX14 has a higher affinity (K_d 323 nM) to CEP55 than ALIX (or TSG101) (K_d 1–3 μM). However, the high affinity itself might not be sufficient to completely prevent the recruitment of ALIX (or TSG101) to CEP55-EABR if the proteins are recruited at the same time.

Consistent with this view, cell biology studies by other groups have previously shown that the order of recruitment to the midbody in germ cells is MKLP1→TEX14→CEP55, whereas that in somatic cells is MKLP1→CEP55→ALIX (or TSG101) (17). In this model, TEX14 is recruited to the midbody before ALIX or TSG101 in germ cells without the help of CEP55-EABR, making the local concentration of the TEX14_{792–804} peptide in the midbody much higher than that of ALIX and TSG101 peptides, which would be favorable for the dominant binding of TEX14_{792–804} to CEP55-EABR. Based on this model, we expected that the CEP55-EABR–TEX14

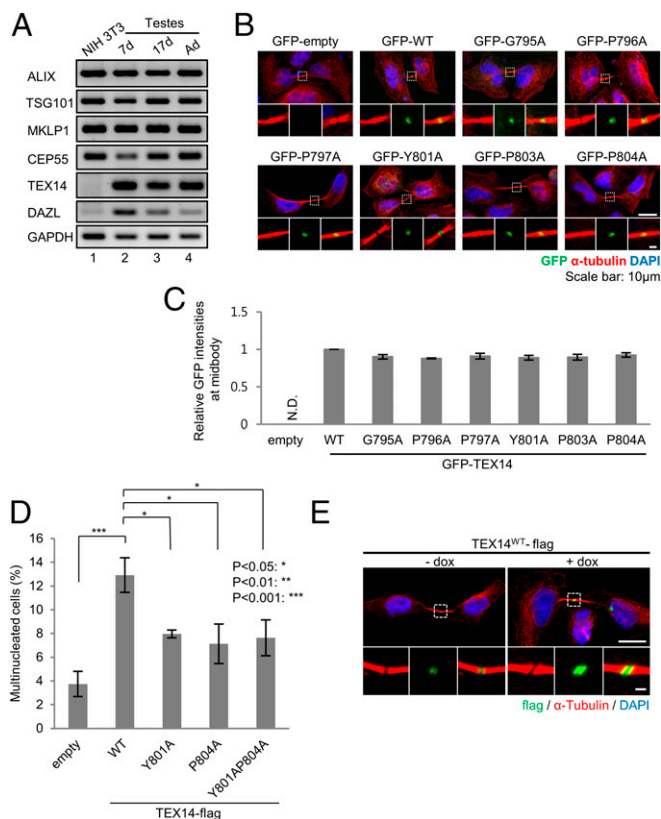


Fig. 4. Effects of point mutations in TEX14 on midbody localization and multinucleation. (A) RT-PCR analysis of ALIX, TSG101, MKLP1, CEP55, and TEX14 expression in both somatic cells and mouse testes. qRT-PCR analysis was additionally performed to determine the relative expression levels of ALIX, TSG101, MKLP1, CEP55, and TEX14 in mouse testes (Fig. S4C). DAZL was used as a marker for male germ cells, and GAPDH was used as an internal control. (B) Midbody localization of wild-type TEX14 and mutants. GFP-TEX14 WT and its mutants were transiently transfected into HeLa cells. All midbody arrested HeLa cells were stained with GFP (green), α -tubulin (red), and DAPI (blue). (Insets) Enlarged views from dashed-line boxes. [Scale bars, 10 μ m; 1 μ m (Insets).] (C) Quantification of GFP intensities at the midbody from the experiment shown in B. A total of 150 midbody arrested cells was counted in three repeated experiments. The relative GFP intensities were normalized by mean intensities of GFP from TEX14 WT transfected cells. Error bars represent SEM. N.D., not determined. (D) Percentages of multinucleated cells containing 2n, 4n, and 8n DNA in wild-type and mutant TEX14-flag stable cell lines ($n = 3$; cell numbers >200 per condition). Error bars represent SEM. (E) Representative microscopic images for TEX14 WT-flag stable cells without doxycycline (-dox) and with 1 μ g/mL doxycycline (+dox). Both midbody arrested stable cells were stained with GFP (green), α -tubulin (red), and DAPI (blue). (Insets) Enlarged views from dashed-line boxes. [Scale bars, 10 μ m; 1 μ m (Insets).]

interaction might not affect the localization of TEX14. Another region of TEX14 may contribute to TEX14 recruitment in the midbody, increasing the local concentration of the TEX14₇₉₂₋₈₀₄ peptide. Therefore, we examined whether the interference of mutations altering CEP55-EABR-TEX14 binding affects the localization of TEX14 to the midbody. We performed an ectopic expression analysis with GFP-TEX14 in HeLa cells and determined subcellular localization. The results show that the wild type and point mutants of GFP-TEX14 are recruited to the midbody without the help of CEP55-EABR (Fig. 4 B and C), consistent with the proposal that TEX14 is recruited to the midbody by binding to MKLP1 before binding to CEP55 in germ cells (17).

To avoid a masking effect due to ectopic overexpression of TEX14, we generated TEX14 stable cell lines. The basal expression of wild-type TEX14 was reduced but, even in the absence of doxycycline, a low level of leaky TEX14 expression was

still detected (Fig. 4E) and the flag-tagged wild-type and mutant TEX14 were expressed stably at similar levels (Fig. 5A). Using wild-type and mutant TEX14 stable cell lines, we monitored the effects of normal cell division by counting multinucleated cells containing 2n, 4n, and 8n DNA (Fig. 4D). The cells expressing wild-type TEX14 were abnormal, exhibiting accumulation of multinucleated intercellular bridges ($P < 0.0001$). These data confirm that TEX14 blocks the recruitment of ESCRT to the midbody. Additionally, TEX14 mutants (Y801A, P804A, and Y801A/P804A) showed significantly reduced percentages of multinucleated cells (7.96%, 7.13%, and 7.64%, respectively; $P < 0.05$) (Fig. 4D). These results suggest that the interaction between CEP55-EABR and TEX14 contributes to the inhibitory role of TEX14 during cell division.

TEX14 Influences the Midbody Displacement of ALIX in Vivo. To investigate whether TEX14 can prevent the recruitment of ALIX to the midbody by competitively binding to CEP55-EABR, we performed ALIX displacement experiments by using wild-type and mutant TEX14 stable cell lines (Fig. 5 A and B). We examined whether it is possible for endogenous ALIX to be localized to the midbody when TEX14 or its mutants are placed in the midbody, assuming that the midbody localization of endogenous ALIX is inhibited upon TEX14 expression. In fact, ALIX

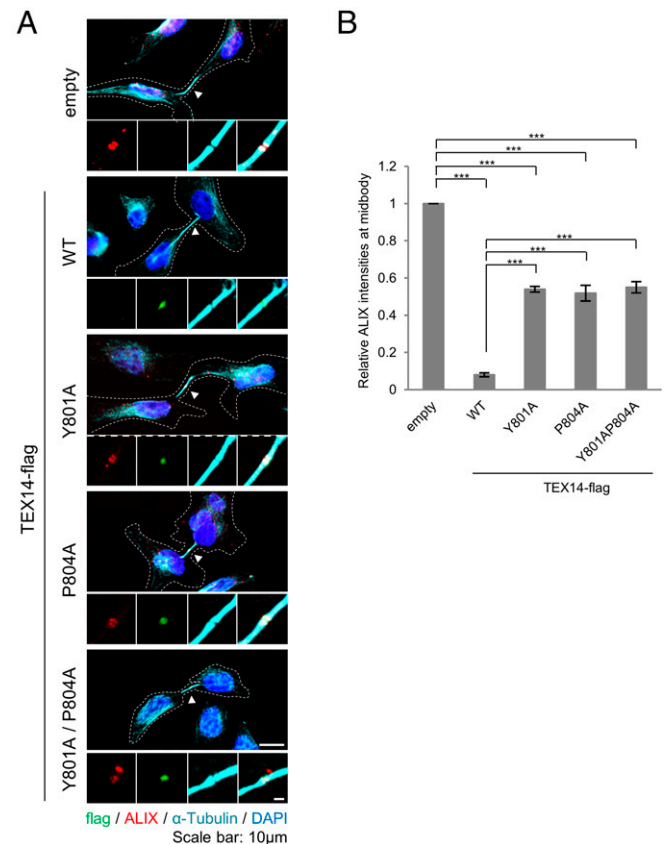


Fig. 5. Midbody displacement of ALIX by TEX14. (A) Representative microscopic images of endogenous ALIX displacement from the midbodies of wild-type TEX14 and mutant stable cells. Stable cells were stained for flag (green), ALIX (red), α -tubulin (cyan), and DAPI (blue). Dotted lines present the outline of midbody arrested cells. Arrowheads indicate the gap at the midbody. (Insets) Enlarged views from dashed-line areas. [Scale bars, 10 μ m; 1 μ m (Insets).] (B) The quantification of ALIX intensities at the midbody from the experiment shown in A. Over 150 midbody arrested cells were counted in each stable cell line, and experiments were repeated three times. The relative ALIX intensities were normalized by mean intensities from empty HeLa FRT/TO cells. Error bars represent SEM. *** $P < 0.0001$.

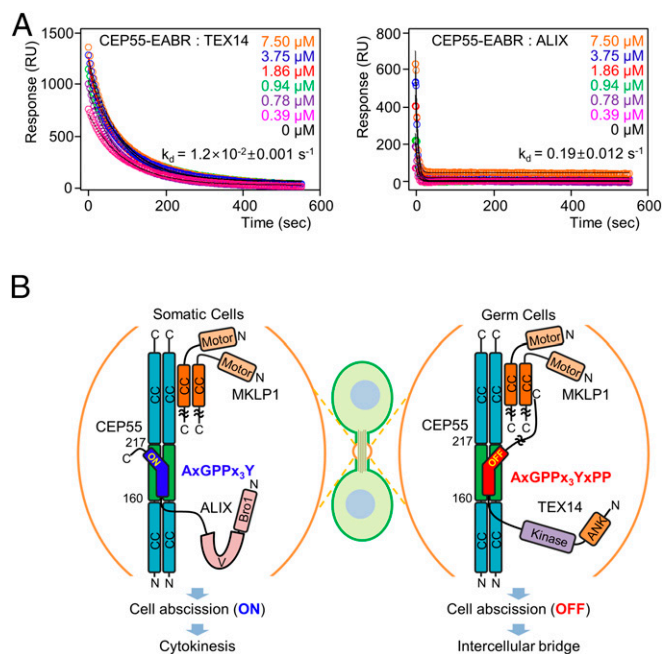


Fig. 6. SPR analysis of CEP55–TEX14 and CEP55–ALIX interactions and an overall model. (A) SPR analysis of dissociation rates of the CEP55–EABR–TEX14 and CEP55–EABR–ALIX interactions. Dissociation curves of bound CEP55–EABR (indicated amounts) from immobilized GST–TEX14_{792–807} or GST–ALIX_{795–811} were measured and fitted to calculate the dissociation rates. (B) A model for the organization of CEP55–TEX14 and CEP55–ALIX complexes in the midbody. Diagram of the multilayered system to safeguard intercellular bridges of germ cells proposed in this study. A schematic of a cell at the midbody stage is drawn, and the domain architectures of CEP55, TEX14, ALIX, and MKLP1 are shown.

is completely displaced when wild-type TEX14 is ectopically expressed (Fig. 5A and B), indicating that TEX14 interrupts the interaction between ALIX and CEP55–EABR. To check the effects of TEX14 mutations, relative fluorescence intensities were compared between wild type and mutants of TEX14 (Fig. 5B). The intensities of endogenous ALIX in the untransfected cells were significantly higher than those of ALIX when wild-type TEX14 was expressed ($P < 0.001$; Fig. 5B). However, when TEX14 mutants (Y801A, P803A, and Y801A/P803A) were expressed, the relative fluorescence intensities of ALIX significantly increased ($P < 0.001$) compared with that of wild-type TEX14 (Fig. 5B). This suggests that the mutation of the AxGPPx₃YxPP motif of TEX14 weakens the binding interaction between TEX14 and CEP55–EABR, resulting in a reduced effect of ALIX displacement.

Longer Residence Time of the TEX14 Peptide Contributes to the Dominant Binding of TEX14 to CEP55–EABR. The ESCRT machinery is necessary for normal abscission of somatic cells, but can act as a potentially damaging membrane scissor for germ cells because intercellular bridges should not be cleaved during spermatogenesis. Therefore, even the binding of a small number of ALIX molecules to CEP55–EABR could be problematic. The higher affinity of the TEX14 peptide to CEP55–EABR and its higher local concentration contribute to its dominant binding. However, the intercellular bridges are still not safe, if the kinetics of binding of the TEX14 peptide to CEP55–EABR is not favorable for its dominant binding. Shorter residence time of TEX14 on CEP55–EABR than that of ALIX may allow the binding of ALIX to CEP55–EABR. To address this, we measured the dissociation rates of the TEX14 and ALIX peptides using SPR (Fig. 6A). The TEX14 peptide dissociated with a rate constant of $0.012 \pm 0.001 \text{ s}^{-1}$, which is ~ 15 times slower than that of the ALIX peptide ($0.19 \pm 0.02 \text{ s}^{-1}$) (Fig. 6A). The longer residence time of the TEX14 peptide ($\sim 80 \text{ s}$) is also favorable for the dominant binding of the TEX14 peptide to CEP55–EABR (Fig. 6A).

Overall Model of Inactivating Germ Cell Abscission and Its Implications.

Taken together, our data demonstrate that the multilayered safeguard system of TEX14 prevents the binding of ALIX (and TSG101) to CEP55–EABR, protecting the intercellular bridges of germ cells from ESCRT machinery, a potentially damaging membrane scissor. Therefore, elucidation of the mechanisms of cell abscission in germ cells, which possess the inherent ability to inactivate cell abscission through TEX14 (Fig. 6B), likely teaches us how to inactivate the abscission of abnormal cells, including cancer cells.

Given the essential role of CEP55 as a regulator of cell abscission through a competitive interplay of TEX14 and ALIX (or TSG101), CEP55 could be an effective target for the artificial control of cytokinesis. CEP55 is one of 70 genes that are implicated in chromosomal instability, and the protein expression of CEP55 is increased in many tumor cells (18). Therefore, CEP55 is thought to be a novel therapeutic target in many disease contexts (17). Accordingly, derivatives of the TEX14 peptide containing the AxGPPx₃YxPP motif of TEX14 could function as a suppressor of cancer cell proliferation by binding to CEP55–EABR and forming stable intercellular bridges.

Consistent with this hypothesis, a previous study demonstrated that it was possible to convert midbodies of somatic cells into germ cell intercellular bridges by expressing TEX14 (19, 20). Although much remains to be learned about the molecular architecture and precise stereochemistry of the intercellular bridge, the results and model presented here provide one foothold for furthering such an understanding.

Materials and Methods

Crystallization and Data Collection. Before crystallization, CEP55_{160–217} protein (7 mg mL^{-1}) in 20 mM Tris–HCl (pH 7.4), 100 mM NaCl and TEX14 peptide (29 mg mL^{-1}) in 150 mM Tris–HCl (pH 8.0) were mixed in a 1:20 volume ratio and incubated at 4 °C for 1 h (Tables S2–S4). Crystals of the CEP55_{160–217}–TEX14_{792–804} complex were grown at 22 °C using sitting-drop vapor diffusion by mixing 1 μL of the protein complex solution with 1 μL of 0.1 M imidazole (pH 8.0), 1 M ammonium phosphate dibasic. Crystals were cryoprotected by soaking in 30% (vol/vol) glycerol solution and flash-frozen in liquid nitrogen. X-ray diffraction data were collected at 100 K in 1° oscillations at beamline 7A of the Pohang Light Source (PLS BL-7A; Pohang Accelerator Laboratory). Raw data were processed and scaled using the HKL-2000 program suite (21). Table S1 summarizes the statistics of data collection. The CEP55_{160–217}–TEX14_{792–804} complex crystal belonged to space group P2₂1₂1, with unit cell parameters of $a = 53.9 \text{ \AA}$, $b = 102.6 \text{ \AA}$, and $c = 132.5 \text{ \AA}$ (Table S1). Crystallization and data collection of the CEP55_{160–217}–TEX14^N–ALIX^C complex and the CEP55_{160–217}–ALIX^N–TEX14^C complex involved steps similar to those used for the CEP55_{160–217}–TEX14_{792–804} complex. Crystals of the CEP55_{160–217}–TEX14^N–ALIX^C complex were produced using 20% (wt/vol) polyacrylic acid 5100, 0.2 M magnesium chloride, 0.1 M 4-(2-hydroxyethyl)-1-piperazineethanesulfonic acid (Hepes) (pH 7.5), and crystals of the CEP55_{160–217}–ALIX^N–TEX14^C complex using 0.8 M ammonium sulfate, 0.1 M sodium citrate (pH 5.0). Crystals of the CEP55_{160–217}–TEX14^N–ALIX^C complex and the CEP55_{160–217}–ALIX^N–TEX14^C complex were cryoprotected by soaking in 25–30% glycerol solution and flash-frozen in liquid nitrogen for data collection.

Structure Determination and Refinement. The structures of the CEP55_{160–217}–TEX14_{792–804} complex, CEP55_{160–217}–TEX14^N–ALIX^C complex, and CEP55_{160–217}–ALIX^N–TEX14^C complex were solved by the molecular replacement method using the dimer model of human CEP55_{160–217} [Protein Data Bank (PDB) ID code 3E1R]. A cross-rotational search followed by a translational search was performed using the Phaser program (22). Subsequent manual model building was carried out using the Coot program (23), and restrained refinement was performed using the REFMAC5 program (24). Several rounds of model building, simulated annealing, positional refinement, and individual B-factor refinement were performed. Table S1 lists the refinement statistics. The crystallographic asymmetric unit of the CEP55_{160–217}–TEX14_{792–804} complex contains four homodimers of the CEP55 peptide and four TEX14 peptides, where chains A, B, D, E, G, H, J, and K correspond to CEP55_{160–217}, and chains C, F, I, and L correspond to the TEX14 peptide. The refined model includes 188 water molecules, and 98.8% of the residues are in the most-allowed region of the Ramachandran plot. No electron density is observed for residues 212–217 in chain A, residues 160–167 and 212–217 in chains B and J, residues 210–217 in chains D and E, residues 211–217 in chain G, residues 209–217 in chain H, and residues 160–165 and 209–217 in chain K of CEP55_{160–217}. Atomic

coordinates and structure factors for the CEP55¹⁶⁰⁻²¹⁷-TEX14⁷⁹²⁻⁸⁰⁷ complex, CEP55¹⁶⁰⁻²¹⁷-TEX14^N-ALIX^C complex, and CEP55¹⁶⁰⁻²¹⁷-ALIX^N-TEX14^C complex have been deposited in the Protein Data Bank (PDB ID codes 3WUJ, 3WUU, and 3WUV, respectively).

Competition Assay. For the competition assay, 350 μ g of CEP55¹⁶⁰⁻²¹⁷ was incubated with TEX14 peptides (20, 40, 160, or 250 μ g) for 1 h at 4 °C. GST-ALIX⁷⁹⁵⁻⁸¹¹ was bound to glutathione-Sepharose beads (GE Healthcare), and a mixture of CEP55¹⁶⁰⁻²¹⁷ and TEX14 peptides was then added and incubated for 1 h. The beads were washed extensively with 20 mM Tris (pH 7.4), 100 mM NaCl. Bound proteins were eluted, separated by SDS polyacrylamide gel electrophoresis (SDS/PAGE), and stained with Coomassie Brilliant Blue.

GST Pull-Down Assay. GST-TEX14^N-ALIX^C and GST-ALIX^N-TEX14^C fusion proteins were bound to glutathione-Sepharose beads (GE Healthcare). CEP55¹⁶⁰⁻²¹⁷ protein was incubated with GST (labeled as TEV), GST-TEX14^N-ALIX^C (labeled as No TEV), or GST-ALIX^N-TEX14^C (labeled as No TEV) for 1 h at 4 °C with gentle shaking in 20 mM Tris-HCl (pH 7.4) containing 100 mM NaCl. After extensive washing, bound proteins were eluted with elution buffer (30 mM glutathione, 150 mM Tris-HCl, pH 8.0), separated by SDS/PAGE, and stained with Coomassie Brilliant Blue.

NMR Spectroscopy. Uniformly ¹⁵N-labeled human CEP55¹⁶⁰⁻²¹⁷ (pGST2, residues 160–217) was expressed by growing *Escherichia coli* BL21(DE3) cells in minimal medium supplemented with ¹⁵NH₄Cl as the sole nitrogen source and inducing expression with 0.5 mM isopropyl β -D-1-thiogalactopyranoside (IPTG) for 18 h at 20 °C. The proteins were purified using GST-affinity and size-exclusion chromatography. The NMR titration experiments were performed with uniformly ¹⁵N-labeled CEP¹⁶⁰⁻²¹⁷ using 600- μ L samples (200 μ M protein, 50 mM Tris-HCl, pH 7.2, 10% D₂O) at 298 K on a Bruker Avance 600 spectrometer equipped with a cryoprobe. The ¹H-¹⁵N transverse relaxation optimized spectroscopy (TROSY) spectra of ¹⁵N-labeled CEP¹⁶⁰⁻²¹⁷ alone or with TEX14 (or ALIX) peptides (50 and 100 μ M) were processed and analyzed with TopSpin (versions 1.3 and 3.0; Bruker). NMR spectra could not be collected for the sequential assignment of CEP55¹⁶⁰⁻²¹⁷ alone, the CEP55¹⁶⁰⁻²¹⁷-TEX14 complex, and CEP55¹⁶⁰⁻²¹⁷-ALIX complex, because a uniformly ¹⁵N, ¹³C-labeled CEP55¹⁶⁰⁻²¹⁷ construct (1 mM) in 20 mM Tris-HCl (pH 7.2), 10% D₂O tended to aggregate during the measurement.

Reverse Transcription and Quantitative Real-Time PCR. All laboratory mice (C57BL/6) were cared for and experimentally used under approval of the Institutional Animal Care and Use Committee at Seoul National University. In this study, testes from adult (7 wk) and 7-d- and 17-d-postpartum mice were used for PCR. Total RNA was extracted from mouse testes on postnatal days 7, 17, and 42 using TRIzol Reagent (Invitrogen). Reverse transcription was performed with random hexamers. Real-time PCR was carried out with the gene-specific primers listed in Table S5. Relative gene expression levels were calculated using the comparative Ct method (25) and normalized to the expression of *GAPDH*.

Surface Plasmon Resonance. Binding of the wild-type and mutant CEP55¹⁶⁰⁻²¹⁷ constructs and TEX14 peptides was measured with a ProteOn XPR36 system (Bio-Rad) at 25 °C with a flow rate of 100 μ L/min. GST-TEX14⁷⁹²⁻⁸⁰⁷ (wild-type, G795A, P796A, P797A, Y801A, P803A, and P804A mutants) and GST-ALIX⁷⁹⁵⁻⁸¹¹ were immobilized on a surface via covalent linkage to the N terminus of GST. A GLM chip (Bio-Rad) was activated using 1:1 *N*-hydroxysuccinimide (NHS)/1-ethyl-3-(3-dimethylaminopropyl) carbodiimide (EDC) at a flow rate of 30 μ L/min for 5 min. Each protein sample (10 μ M) in 10 mM acetate buffer (pH 4.5) was passed over separate flow cells at 30 μ L/min for 5 min, followed by a blocking step using ethanolamine (1 M, pH 8.5) at 30 μ L/min for 5 min. All binding experiments were performed in 20 mM Tris (pH 7.5), 100 mM NaCl. Binding of CEP55¹⁶⁰⁻²¹⁷ proteins with wild-type TEX14 was measured by passing CEP55¹⁶⁰⁻²¹⁷ (wild-type, W184A, Y187A, R191A, and E192A) over flow cells coupled to GST-TEX14⁷⁹²⁻⁸⁰⁷ with association and dissociation times of 300 and 400 s, respectively. Binding of wild-type ALIX, TEX14 mutants, and chimeric peptides to wild-type CEP55¹⁶⁰⁻²¹⁷ was measured by passing CEP55¹⁶⁰⁻²¹⁷ over flow cells coupled to GST-ALIX⁷⁹⁵⁻⁸¹¹, GST-TEX14⁷⁹²⁻⁸⁰⁷ mutants (G795A, P796A, P797A, Y801A, P803A, and P804A), or GST-chimera peptides (TEX14^N-ALIX^C and ALIX^N-TEX14^C) with association and dissociation times of 300 and 400 s, respectively. Between subsequent injections of all of the proteins, surfaces were regenerated with an injection of 20 mM Tris (pH 7.5), 500 mM NaCl for 10–30 s at 30 μ L/min.

Constructs for Cell Biology and Generation of Stable Cell Lines. The GFP-TEX14 construct was cloned into the *EcoRI/XmaI* sites of the pEGFP-C2 vector (Clontech). Site-directed mutants of GFP-TEX14 (G795A, P796A, P797A, Y801A, P803A, and P804A) were generated using the QuikChange Mutagenesis Kit (Stratagene) and the mutations were verified by DNA sequencing. The genes encoding the wild-type TEX14 and mutants (Y801A, P804A, and Y801A/P804A), which were cleaved from the previously cloned GFP-TEX14 WT and mutant constructs by *HindIII/SmaI*, were inserted into the pcDNA5/TO/FRT/3xflag vector. To establish stable cell lines expressing TEX14 WT and mutants, pcDNA5/TO/FRT/3xflag containing TEX14 and POG44 was mixed at a 1:9 ratio and transfected into HeLa FRT/TO cells with FuGENE following the manufacturer's protocol (Roche). Selections were conducted with hygromycin (50 mg/mL) to collect surviving colonies. Established stable cell lines were maintained in DMEM supplemented with 10% FBS at 37 °C in a 5% CO₂ incubator. To induce TEX14 expression, the cells were treated with doxycycline (1 μ g/mL).

ACKNOWLEDGMENTS. The authors thank the staff at beamline 7A of the Pohang Light Source for their assistance with X-ray experiments. This study was supported by a grant from the National Research Foundation of Korea funded by the Korean government (2013R1A1A1A1008195 and 2015R1A5A1A008958) and a grant from the Korea Carbon Capture & Sequestration R&D Center (KCRC; 2013M1A8A1038187) (to H.H.L.).

- Greenbaum MP, Iwamori T, Buchold GM, Matzuk MM (2011) Germ cell intercellular bridges. *Cold Spring Harb Perspect Biol* 3(8):a005850.
- Greenbaum MP, et al. (2006) TEX14 is essential for intercellular bridges and fertility in male mice. *Proc Natl Acad Sci USA* 103(13):4982–4987.
- Rustom A, Saffrich R, Markovic I, Walther P, Gerdes HH (2004) Nanotubular highways for intercellular organelle transport. *Science* 303(5660):1007–1010.
- Dubey GP, Ben-Yehuda S (2011) Intercellular nanotubes mediate bacterial communication. *Cell* 144(4):590–600.
- McLean PF, Cooley L (2013) Protein equilibration through somatic ring canals in *Drosophila*. *Science* 340(6139):1445–1447.
- Hurley JH, Hanson PI (2010) Membrane budding and scission by the ESCRT machinery: It's all in the neck. *Nat Rev Mol Cell Biol* 11(8):556–566.
- Carlton JG, Martin-Serrano J (2007) Parallels between cytokinesis and retroviral budding: A role for the ESCRT machinery. *Science* 316(5833):1908–1912.
- Morita E, et al. (2007) Human ESCRT and ALIX proteins interact with proteins of the midbody and function in cytokinesis. *EMBO J* 26(19):4215–4227.
- Carlton JG, Agromayor M, Martin-Serrano J (2008) Differential requirements for Alix and ESCRT-III in cytokinesis and HIV-1 release. *Proc Natl Acad Sci USA* 105(30):10541–10546.
- Hanson PI, Roth R, Lin Y, Heuser JE (2008) Plasma membrane deformation by circular arrays of ESCRT-III protein filaments. *J Cell Biol* 180(2):389–402.
- Stuchell-Brereton MD, et al. (2007) ESCRT-III recognition by VPS4 ATPases. *Nature* 449(7163):740–744.
- Wollert T, Wunder C, Lippincott-Schwartz J, Hurley JH (2009) Membrane scission by the ESCRT-III complex. *Nature* 458(7235):172–177.
- Wollert T, Hurley JH (2010) Molecular mechanism of multivesicular body biogenesis by ESCRT complexes. *Nature* 464(7290):864–869.
- Chung CC, et al. (2013) Meta-analysis identifies four new loci associated with testicular germ cell tumor. *Nat Genet* 45(6):680–685.
- Lee HH, Elia N, Ghirlando R, Lippincott-Schwartz J, Hurley JH (2008) Midbody targeting of the ESCRT machinery by a noncanonical coiled coil in CEP55. *Science* 322(5901):576–580.
- Wu WJ, Raleigh DP (1998) Local control of peptide conformation: Stabilization of *cis* proline peptide bonds by aromatic proline interactions. *Biopolymers* 45(5):381–394.
- Iwamori T, Lin YN, Ma L, Iwamori N, Matzuk MM (2011) Identification and characterization of RBM44 as a novel intercellular bridge protein. *PLoS One* 6(2):e17066.
- Sakai M, et al. (2006) Elevated expression of C10orf3 (chromosome 10 open reading frame 3) is involved in the growth of human colon tumor. *Oncogene* 25(3):480–486.
- Greenbaum MP, Ma L, Matzuk MM (2007) Conversion of midbodies into germ cell intercellular bridges. *Dev Biol* 305(2):389–396.
- Iwamori T, et al. (2010) TEX14 interacts with CEP55 to block cell abscission. *Mol Cell Biol* 30(9):2280–2292.
- Otwinowski Z, Minor W (1997) Processing of X-ray diffraction data collected in oscillation mode. *Methods Enzymol* 276:307–326.
- McCoy AJ, Grosse-Kunstleve RW, Storoni LC, Read RJ (2005) Likelihood-enhanced fast translation functions. *Acta Crystallogr D Biol Crystallogr* 61(4):458–464.
- Emsley P, Cowtan K (2004) Coot: Model-building tools for molecular graphics. *Acta Crystallogr D Biol Crystallogr* 60(12):2126–2132.
- Murshudov GN, Vagin AA, Dodson EJ (1997) Refinement of macromolecular structures by the maximum-likelihood method. *Acta Crystallogr D Biol Crystallogr* 53(3):240–255.
- Schmittgen TD, Livak KJ (2008) Analyzing real-time PCR data by the comparative CT method. *Nature Protocols* 3(6):1101–1108.
- Sheffield P, Garrard S, Derewenda Z (1999) Overcoming expression and purification problems of RhoGDI using a family of “parallel” expression vectors. *Protein Expr Purif* 15(1):34–39.